

Fabrication of Diamond Nanowires for Quantum Information Processing Applications

Birgit J. M. Hausmann^{a,b}, Mughees Khan^a, Yinan Zhang^a, Tom M. Babinec^a, Katie Martinick^c, Murray McCutcheon^a, Phil R. Hemmer^d, Marko Lončar^a

^a*School of Engineering and Applied Sciences, Harvard University, McKay Lab 219, 9 Oxford Street, Cambridge MA, 02138, United States*

^b*Department of Physics, Technische Universität München, James Franck Str., D-85748 Garching, Germany*

^c*Department of Chemical and Nuclear Engineering, The University of New Mexico, 1 University of New Mexico, Albuquerque, NM 87131-0001, United States*

^d*Department of Electrical and Computer Engineering, Texas A&M University, 216H Zachry, TAMU 3128 College Station, Texas 77843-3128, United States*

Abstract

We present a design and a top-down fabrication method for realizing diamond nanowires in both bulk single crystal and polycrystalline diamond. Numerical modeling was used to study coupling between a Nitrogen Vacancy (NV) color center and optical modes of a nanowire, and to find an optimal range of nanowire diameters that allows for large collection efficiency of emitted photons. Inductively coupled plasma (ICP) reactive ion etching (RIE) with oxygen is used to fabricate the nanowires. Drop-casted nanoparticles (including Au, SiO₂ and Al₂O₃) as well as electron beam lithography defined spin-on glass and evaporated Au have been used as an etch mask. We found Al₂O₃ nanoparticles to be the most etch resistant. At the same time FOX e-beam resist (spin-on glass) proved to be a suitable etch mask for fabrication of ordered arrays of diamond nanowires. We were able to obtain nanowires with near vertical sidewalls in both polycrystalline and single crystal diamond. The heights and diameters of the polycrystalline nanowires presented in this paper are $\approx 1\ \mu\text{m}$ and 120 – 340 nm, respectively, having a 200 nm/min etch rate. In the case of single crystal diamond (types Ib and IIa) nanowires the height and diameter for different diamonds and masks shown in this paper were 1 – 2.4 μm and 120 – 490 nm with etch rates between 190 – 240 nm/min.

Key words: Diamond, Nanowire, Reactive ion etching, ICP, Nanostructure

1. Introduction

Nitrogen-vacancy (NV) color centers embedded in diamond have recently emerged as a promising platform for the realization of robust, room temperature, single-photon sources [1]. The NV center is formed by a two point defect in the diamond lattice: A substitutional nitrogen atom and a vacancy (missing carbon atom) trapped at an adjacent lattice position. It can exist in two charged states NV⁰ and NV⁻ out of which the NV⁻ center is suitable for quantum operations due to the electron's spin kinetics. The luminescence spectrum of an NV⁻ color center consists of a broad (640 nm to 780 nm) phonon side-band (PSB) and a zero-phonon line (ZPL) at 637 nm [2, 3]. NV centers combine the key advantages of isolated atomic systems with solid-state integration, and have the following unique optical properties: (i) room temperature operation, (ii) little inhomogeneous broadening and (iii) deterministic positioning using ion implantation. Moreover, the NV center stands out among solid state systems because its electronic spin can be prepared, manipulated, and measured with optical and microwave excitations [4].

However, NV centers also interact with their environment leading to decoherence in the presence of nearby nitrogen spins. Hence it is important to enhance the NV center emission yield (photon production rate) as well as increase the collection efficiency of emitted photons. This can be achieved by embedding NV centers within optical structures including cavities, microdisks, waveguides and nanowires.

NV⁻ optical transition is in the visible (637 nm), which limits the choice of materials that can be used to realize optical structures. Diamond itself is a suitable platform having a reasonably high refractive index ($n = 2.43$). Baldwin et al. [5] have fabricated 2D photonic crystal (PhC) slabs in polycrystalline diamond (poly-D) on insulator (DOI) films. Similarly, Wang et al. [6, 7] have demonstrated the fabrication of optical microdisk resonators and 2D PhC in polycrystalline diamond films using E-Beam Lithography (EBL) and Reactive Ion Etching (RIE). The characterization of poly-D microdisks and photonic crystal cavities has shown scattering losses due to the polycrystalline nature of the diamond film. Moreover, the emission from polycrystalline diamond itself can obscure single-photon emission from an embedded NV center. Hence, defect-free single crystal diamond (sc-D) films are needed for Quantum Information Processing (QIP) applications.

*Corresponding author: Tel.: +1 617 2300238

Email address: hausmann@seas.harvard.edu (Birgit J. M. Hausmann)

High-quality sc-D films can only be homo-epitaxially grown on the diamond substrate and therefore the needed index contrast for the realization of nanophotonic devices does not exist. Olivero et al. [8] have used ion-beam implantation followed by sacrificial removal of implanted graphitized (damaged) layer to fabricate thin sc-D films. Based on this approach fabrication of sc-D waveguides [9] and microdisk resonators [10] has been demonstrated. However, the ion implantation may create additional NV centers and may render such thin films unsuitable for QIP applications.

Optical structures fabricated in a GaP layer bonded on top of a diamond film [11] have also been reported. Approaches based on diamond nanocrystals containing NV centers embedded within a silicon-nitride photonic crystal structure has been examined theoretically [12]. Other works include positioning diamond nanocrystals on top of wide bandgap materials such as GaP [13] and silicon-dioxide [14] as well as metallic nanostructures [15].

In this work an alternative approach has been explored based on the fabrication of nanowires in diamond containing NV centers. Recently, Friedler et al. [16] have theoretically demonstrated a 90% extraction efficiency of emitted photons from single-photon sources like quantum dots embedded within semiconductor nanowires. We first examine an optimal nanowire diameter that maximizes the overall collection efficiency of photons emitted from an NV center. Next, we developed a fabrication procedure for the creation of diamond nanowires directly in high-quality sc-D substrates utilizing RIE and as needed EBL. Our procedure uses oxygen as a reactive gas in an inductively coupled plasma (ICP) RIE. In the past a two step procedure for diamond nano-rods based on hydrogen treated sc-D whiskers has been pursued [17]. Other fabricated structures in poly- and sc-D based on reactive ion etching (RIE) include microlenses [18, 19], porous diamond [20], field emitters [21], waveguides [9], atomic force microscopy (AFM) tips [22], disks [10], cones and cylinders [23], nanopillars [24], micro-cylinders [25] and resonator arrays for RF signal processing [26]. As masks, we investigated two main approaches: (i) nanoparticles deposited using drop-casting (Au, SiO₂, Al₂O₃), and (ii) masks defined by EBL using positive as well as negative resist. We also investigated two types of substrates: (i) poly-D films on insulator, and (ii) sc-D diamonds grown via high-pressure high-temperature (HPHT) and chemical vapor deposition (CVD) processes.

2. Design and Modeling

First, we studied the emission from an NV center (modeled as a dipole) in a diamond nanowire using FDTD simulations. We assume a circular cross section of the nanowire with a diameter d , and consider the two general polarization scenarios for a dipole/nanowire system: dipole polarization perpendicular (s-polarized) and parallel (p-polarized) to the nanowire axis. The dipole associated with an NV center in (100) diamond can be rep-

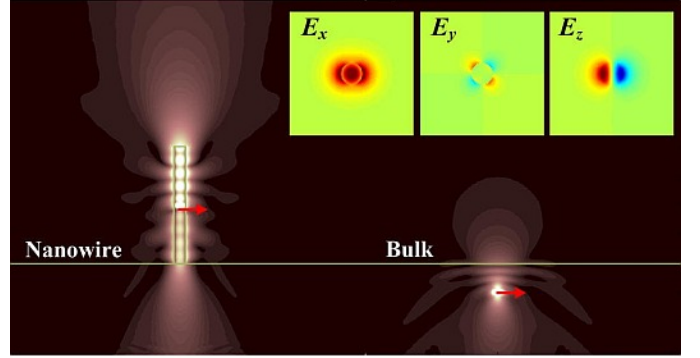


Figure 1: Field profile of the E-field's radial component (E_r) in the case of a $2\mu\text{m}$ long, 200 nm diameter diamond nanowire (left) and a bulk diamond (right). The dipole is polarized parallel to the interface, emitting at $\lambda = 637\text{ nm}$ (zero-phonon line wavelength of NV center). The fundamental nanowire waveguide mode (HE_{11}) (inset) is the dominant decay channel for the nanowire case.

resented using combination of these two dipoles, since it is polarized in the (111) plane. At different wavelengths within the NV center's radiation spectrum ($637\text{ nm} - 780\text{ nm}$), the number of collected photons per second can be expressed as $\Gamma(\lambda) \cdot \eta(\lambda)$ where Γ is the emission rate (reciprocal to the lifetime) and η the collection efficiency. The collection efficiency can be dramatically improved in diamond nanowires compared with bulk diamond, as demonstrated in Figure 1. These field profiles show that the major portion of light emitted from an NV center in bulk diamond leaks to the substrate due to significant total internal reflection at the diamond-air interface, whereas in a diamond nanowire the fundamental HE_{11} mode is the dominant emission channel for a dipole polarized perpendicular to the nanowire axis (in the xy plane) (Fig. 1, inset) [16]. This waveguide mode directs the light propagating in the nanowire, and is scattered vertically as it exits from the top nanowire facet. This process allows for efficient collection using an objective lens positioned above [27]. In Figure 2a we show the coupling efficiency, α , between the NV center and the nanowire waveguide mode as a function of the nanowire diameter, for wavelength $\lambda = 637\text{ nm}$. It can be seen that, in the case of s-polarized dipole, more than 80% of emitted photons can couple to the nanowire mode for a broad range of nanowire diameters ($180\text{ nm} - 230\text{ nm}$). We choose to work with 200 nm diameter nanowires in order to optimize the coupling efficiency. Photon collection efficiencies can be quantified from the far-field profile of power emitted upward, shown in Figure 2b and c. An objective lens with a numerical aperture $\text{NA}=0.95$, positioned above the nanowire, can collect light emitted into the solid angle of 72° (represented by shaded areas in the far field emission profiles). It can be seen that in the case of both s- and p-polarized dipoles, almost 100% of photons emitted from the nanowire can be collected with the lens. It is interesting to note that this is true even for p-

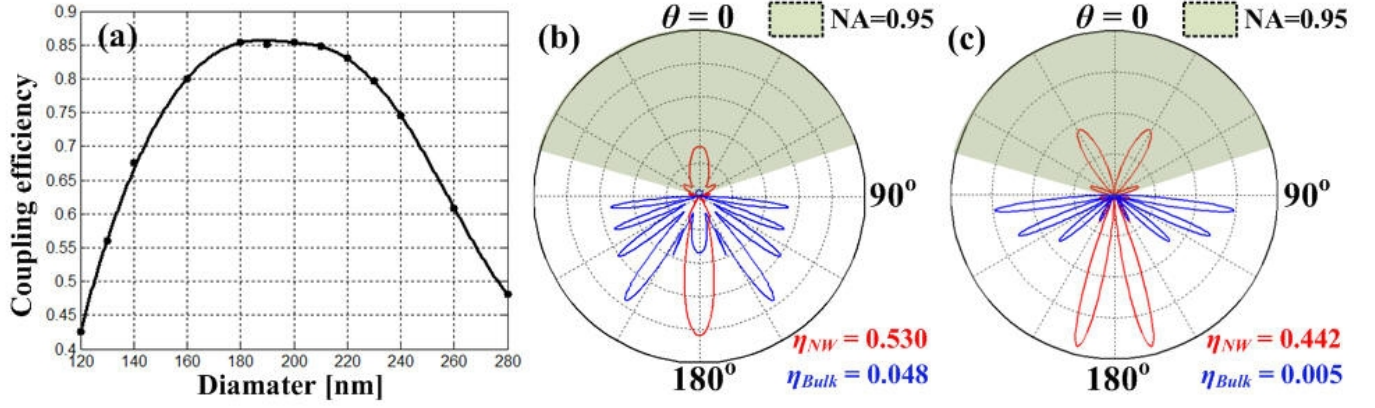


Figure 2: (a) Coupling efficiency α as a function of the nanowire diameter at $\lambda = 637$ nm. The dipole is assumed to be placed at the center of the nanowire with a polarization perpendicular to the nanowire axis (s-polarized). (b) and (c): The far-field profile of power emitted from a (b) s-polarized and (c) p-polarized (parallel to the nanowire axis) dipole embedded at the center of a nanowire with $d = 200$ nm. Blue lines, in both (b) and (c), show far-field profiles of emitter embedded in the bulk diamond crystal. The shaded areas denote the light that can be collected using an objective lens with an NA of 0.95. Calculated values of collection efficiency η for nanowire and bulk, for both polarizations, are also indicated.

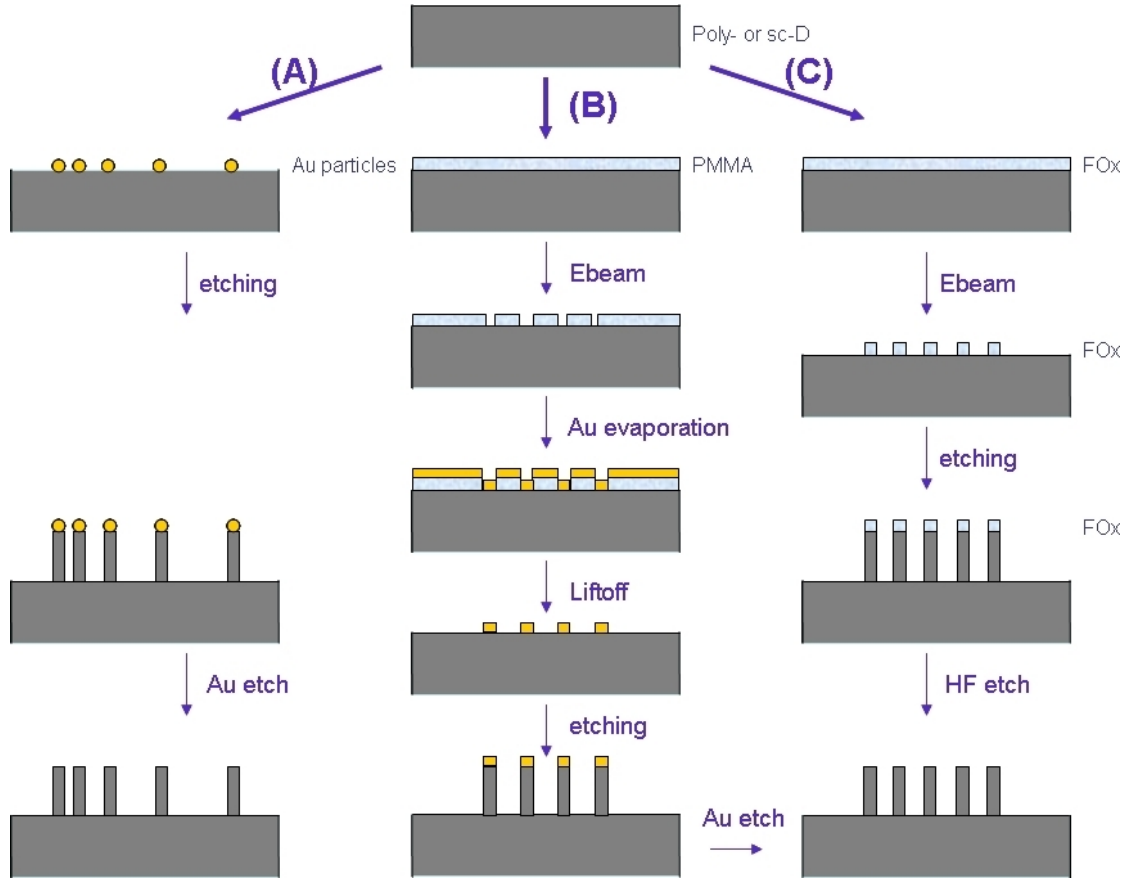


Figure 3: Fabrication process schematic. (A): Drop casting of nanoparticles (Al₂O₃, Au, SiO₂) followed by etching. (B) EBL defined Au evaporation and etching. (C) EBL defined FOx mask (flowable oxide, a spin-on-glass resist) and etching.

polarized dipole despite the fact that it cannot couple to the nanowire waveguide mode due to the symmetry mismatch. In this case, however, large collection efficiency is enabled by coupling to radiative modes that are also modified by the presence of the nanowire. Finally, comparing a dipole in a nanowire (red line in figures 2b and c) with a dipole in a bulk diamond crystal (blue line), we find that the nanowire geometry provides one and two orders of magnitude improvement in the collection efficiency in the case of s-polarized and p-polarized dipole, respectively. We also evaluated the total emission rate (the reciprocal of lifetime) of an NV center in a nanowire, and found that it is dependent on the NV's position: Fabry-Perot resonances, formed due to the (weak) reflection of a waveguide mode from the nanowire's facets, can modify the emission rate of s-polarized dipole. We introduce the enhancement factor $E(\lambda) = \frac{\Gamma(\lambda)}{\Gamma_0(\lambda)}$ where Γ_0 is the emission rate of the quantum emitter in a homogeneous diamond medium. For $\lambda = 637\text{nm}$ and $d = 200\text{nm}$, the enhancement factor is in the range of 0.65 – 1.10, depending on the dipole position along the nanowire positions. It is interesting to note that the collection efficiency for s-polarized dipole is maximized (Figure 2b) when destructive interference occurs between downward emitted photons and photons reflected from the top nanowire facet (Figure 1). This case favors upward emission at the expense of slightly increased radiative lifetime.

In order to estimate the total number of photons that can be collected from a nanowire geometry, it is important to take into account both s- and p-polarized components of NV dipole, as well as its broad-band emission due to the phonon sideband. The total number of collected photons is obtained by averaging over wavelengths and polarizations, by using following (unitless) figure of merit

$$Z = \frac{\int \int E(\lambda, \sigma) \eta(\lambda, \sigma) \Gamma_0(\lambda) d\sigma d\lambda}{2\pi \int \Gamma_0(\lambda) d\lambda}$$

where σ denotes the polarization angle.

Using this figure of merit, we find that the nanowire geometry provides an order of magnitude improvement ($Z \approx 30\%$) over the bulk diamond case ($Z \approx 3.3\%$).

3. Materials and Methods

We used two types of diamond samples based on their crystalline nature: a) poly-D films and b) type Ib and IIa sc-Ds synthesized via HPHT and CVD processes respectively. While sc-Ds are needed to realize single-photon sources, poly-d films have been used to optimize the etch recipe due to their low-cost and availability in large quantities.

The poly-D samples were diamond on insulator (DOI) AQUA 25 wafers ($2\mu\text{m}$ poly-D film on $1\mu\text{m}$ thermal SiO_2 on a Si substrate) from Advanced Diamond Technologies, Inc. The sample size was about $3 - 5\text{mm} \times 3 - 5\text{mm}$.

Prior to mask deposition and reactive ion etching all poly-D samples were solvent cleaned. The nitrogen rich HPHT Ib and very pure (nitrogen content $< 0.1\text{ppm}$) CVD IIa sc-Ds were obtained from Element6 (E6), and were $3\text{mm} \times 3\text{mm}$ in size. We also used a CVD sc-D from Apollo Diamond, Inc. All sc-D samples had a $\langle 100 \rangle$ crystal orientation and prior to mask deposition, and etching all sc-Ds were cleaned for about 45 min in a boiling 1:1:1 (Nitric : Perchloric : Sulfuric) acid bath. This aggressive etch was not used with the poly-D samples as it was damaging the DOI film.

Three major types of etch masks have been explored in this work, each of which required a slightly different fabrication approach. The adopted fabrication processes are shown in Figure 3. The etch masks were prepared as discussed below.

- (A) Nanoparticle mask, deposited via drop-casting: In this approach drop casted nanoparticles have been used as an etch mask. Au colloids suspended in DI water were obtained from Ted Pella, Inc. The nominal particle sizes were 100 nm and 250 nm. However, our measurements indicated a large variation with mean particle diameters of $\approx 140\text{nm}$ and $\approx 350\text{nm}$ respectively. The concentrations were 5.6×10^9 particles/mL and 3.6×10^8 particles/mL for the 100 nm and 250 nm colloids respectively. Au nanoparticles were further diluted in 1:1 and 1:2 ratio with DI water before dispersing on the samples. A suspension of SiO_2 nanoparticles (Corpuscular, Inc.) with a diameter of $\approx 213\text{nm}$ and a 5% particle concentration in a 10 mL solution was also used. The SiO_2 particle-size variation was smaller than 8%. Finally, Al_2O_3 powder from Alfa Aesar, Inc. with 200 nm and 40–50 nm diameters were used.
- (B) Au mask defined via a lift-off process: In this approach, evaporated Au was used as an etch mask as illustrated in Figure 3. Bilayer PMMA from MicroChem Corp was used to define an etch pattern using a 100 kV Elionix e-beam tool. Dosages were varied from $800\mu\text{C}/\text{cm}^2$ to $1600\mu\text{C}/\text{cm}^2$. Next, 10 nm Cr and 200 nm Au evaporation followed by a lift-off process was used to define a metal etch mask.
- (C) Spin-on-glass (HSQ) mask defined by EBL: Flowable oxide (FOX 17) from Dow Corning was diluted with MIBK in 1:2 and 1:1 ratios. Dosages from $4800\mu\text{C}/\text{cm}^2$ to $8000\mu\text{C}/\text{cm}^2$ were used to expose FOX resist.

An ICP RIE system (UNAXIS shuttleline) was used to transfer the mask pattern into all the diamond samples. An etch recipe having 30 sccm oxygen flow rate, 100 W Bias power, 700 W ICP power at a 10 mTorr chamber pressure was used and will be discussed in the next section. After RIE, gold (type TFA, Transene) and chrome etchant (type 1020, Transene) were used in approaches (A) and (B) to remove the remaining Au/Cr mask. In case (C),

an HF (49%, aq) wet etch was performed to remove the remaining FOx mask.

All images were taken with a Zeiss SUPRA field emission scanning electron microscope (FESEM) under a 86° tilt unless noted otherwise. The secondary electron (SE) detector and an acceleration voltage of 5 kV was used.

4. Results and discussion

4.1. Etch recipe variation

Based on our design presented earlier, an etch recipe and etch mask that yield wires with vertical profile and high selectivity are needed. Several dry etch parameters were varied in order to obtain an acceptable wire profile. The results are presented in Figure 4 and the etch parameter variations, heights and diameters are summarized in Table 1. Waist diameter refers to the thickest part of the nanowire and the taper angle is calculated based on the waist and the bottom diameter. The tabulated variations are for a 5 min etch using Au colloids with a diameter of ≈ 250 nm as an etch mask on poly-D samples. A height of $1\ \mu\text{m}$ was determined in most cases, except for (d) and (g) the height was $1.1\ \mu\text{m}$ and $0.7\ \mu\text{m}$ respectively.

Recipe (a) resulted in unwanted grass. Raising the temperature and decreasing the pressure resulted in smooth bottom surfaces (no grass) but introduced a noticeable mask erosion at the top (b). Further increase in temperature resulted in re-appearance of the grass (c) and a reduced etch depth. Slightly undercut wires are obtained with a higher oxygen flow rate of 45 sccm (recipe d) and a reduced temperature compared to recipe (b) as shown in Figure 4d. The increased flow rate and reduced temperature also increased the mask erosion at the top of the nanowires. To consider the effect of an increased ion density the ICP power was increased by 30% (recipe (e)) while reducing the oxygen flow rate compared to recipe (d) by 33%. This yielded in a 3.5 times larger undercut compared to recipe (d). In recipe (f) (Figure 4f) the chamber pressure was decreased to 3 mTorr, the bias power was increased to 200 W and the oxygen flow rate was reduced to 30 sccm compared to recipe (d) which lead to mask erosion and excessive etching. In Figure 4g the etch recipe with 20 mTorr and 200 W was tested to minimize mask erosion by increasing the pressure compared to recipe (f). This resulted in relatively little mask erosion, an over cut wire profile and a reduced etch depth. To minimize the mask erosion observed in recipe (b) and (d) (Figures 4b, 4d), the oxygen flow rate was reduced to 30 sccm compared to recipe (d) as tabulated in recipe (h). This gave a near vertical wire profile with minimal mask erosion as shown in Figure 4h and was used as the basic recipe for etching all the diamond samples presented in this paper.

4.2. Comparison of nanoparticle etch mask

In order to improve the etch selectivity, different nanoparticle masks were also evaluated. A close up view of poly-D

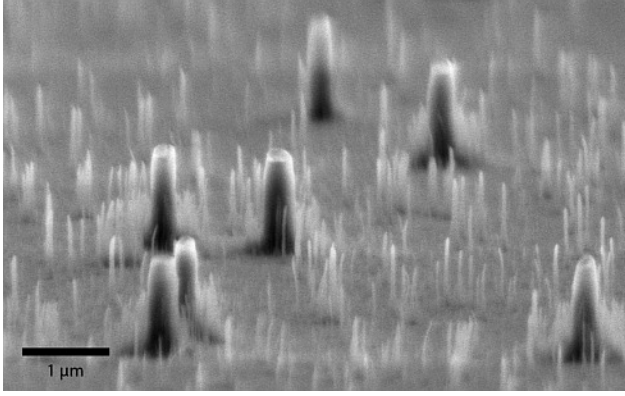
wires obtained using the optimized etch recipe with different nanoparticle masks are shown in Figure 5.

The Al_2O_3 mask was tried first. A similar mask has been used successfully to build micropost-cavities with embedded quantum dots in the past [28]. Al_2O_3 nanoparticles were deposited from both suspension and powder form. In the latter case, the samples were dipped top-down into the powder. Al_2O_3 was found to be an ideal etch mask with no appreciable erosion. A 4 min oxygen etch gave a height of the etched diamond structure of $\approx 1\ \mu\text{m}$ and a diameter of 200 nm both at the top and the bottom, as shown in Figure 5a. The thickest diameter was 230 nm. The particle height was ≈ 210 nm and its thickest diameter was 230 nm. However, Al_2O_3 nanoparticles were found to be clumping together, resulting in large etched features with random cross-sectional profiles (Figure 5a), which was not desirable. Better uniformity and isolation of individual Al_2O_3 nanoparticles can be achieved by modifying the Al_2O_3 nanoparticles deposition process.

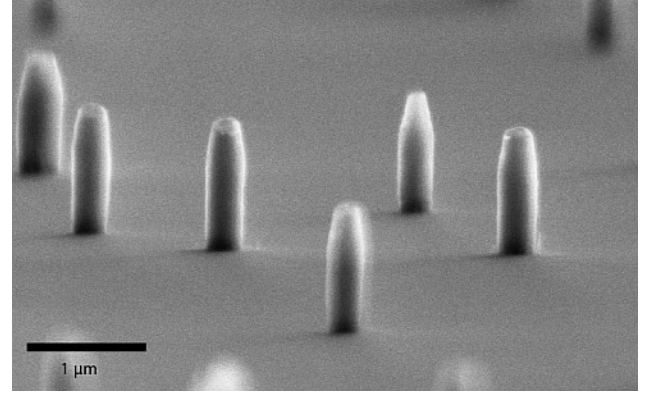
Due to better size and shape uniformity SiO_2 nanoparticles were also evaluated. Figure 5b shows the etch results obtained using individual SiO_2 nanoparticles. Poor selectivity and a high mask erosion were observed, since SiO_2 particles were etched at a rate of ≥ 40 nm/min. The mask erosion also resulted in a tapered nanowire profile. The height of the wires after a 5 min oxygen etch was $1\ \mu\text{m}$, and the diameter varies from ≈ 342 nm on the bottom to ≈ 20 nm at the top. The SiO_2 particles did not survive the etch.

Figure 5c shows a ≈ 900 nm high nanowire obtained with 250 nm gold particles as the mask. The diameter varied from 275 nm on the bottom to a maximum of 310 nm and 250 nm at the top. The particle shown in this image measures 245 nm in diameter and 130 nm in height. The etch time was 5 min.

The Au nanoparticles were the easiest to disperse, resulting in single nanoparticles requiring no further processing stjpg. Using 250 nm nanoparticles, a 5 min etch resulted in $1\ \mu\text{m}$ tall nanowires, as shown in Figure 6a. The diameter varied from 260 nm at the bottom and top to 280 nm as thickest diameter. The etch rates of the mask and the DOI film were determined to be 25 nm/min and 200 nm/min, respectively. This results in an etch selectivity of 8:1. The wires created in poly-D have a near-vertical profile. Figure 6a and Figure 6b show a comparison of poly-D wires etched using 250 nm and 100 nm nanoparticles. The use of 100 nm Au particles (1:200 dilution) resulted in similar etch rates but with a tapered nanowire profile, which can be attributed to significant mask erosion in the case of the small gold nanoparticles (Figure 6b). However, such tapered profile may be beneficial for achieving high extraction efficiency for photons emitted from NV centers embedded within nanowires [16], [29]. The height was $\approx 0.9\ \mu\text{m}$ and the thickest diameter is about 120 nm.



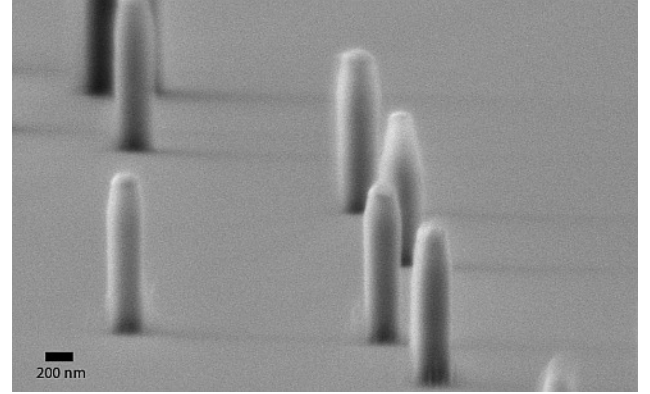
(a)



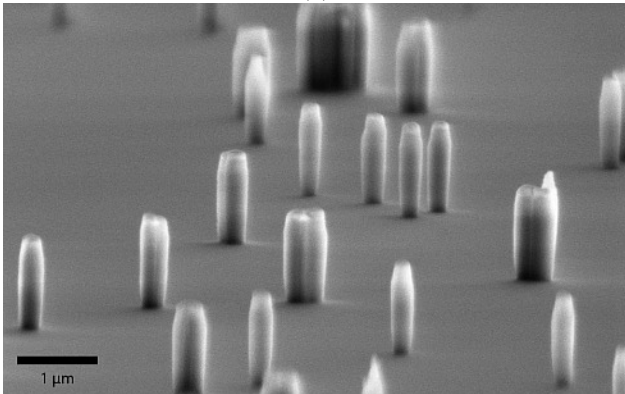
(b)



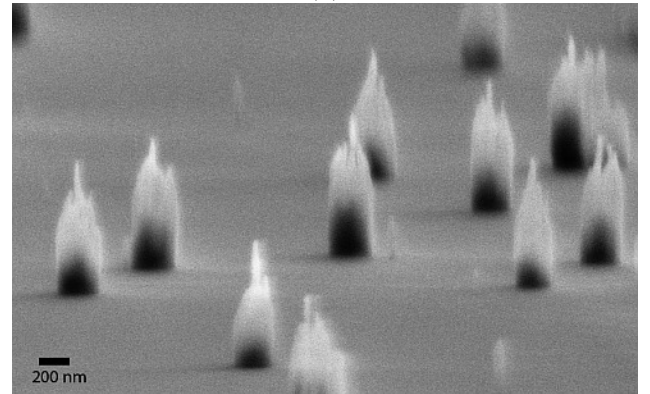
(c)



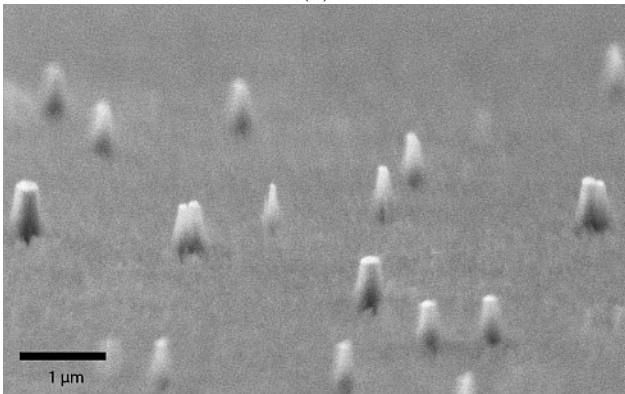
(d)



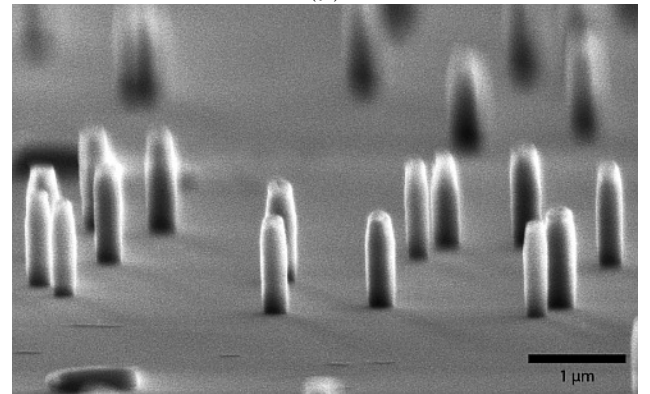
(e)



(f)



(g)



(h)

Figure 4: Summary of etch recipe variations in DOI after a 5 min oxygen dry etch, using 250 nm Au particles as mask. Labels (a) through (h) correspond to etch recipes with the same name in Table 1.

Table 1: Summary of all etch variations. Straight wires were obtained with the optimized etch recipe (last row) for poly-D.

Rec.	Temp. °C	Press. mTorr	Bias W	ICP W	O ₂ sccm	etch rate nm/min	Bottom \varnothing nm	Top \varnothing nm	Waist \varnothing nm	Taper angle °	Result
(a)	RT	20	100	700	30	200	330-420	270	330	-	grass
(b)	73	10	100	700	30	200	290	240	330	88	undercut
(c)	132	10	100	700	30	-	-	250	250	-	grass
(d)	RT	10	100	700	45	220	280	220	300	89.5	straight
(e)	RT	10	100	1000	30	200	220	220	310	87.4	undercut
(f)	RT	3	200	700	30	-	280	-	280	-	erosion
(g)	RT	20	200	700	30	140	-	200	-	-	over cut
(h)	RT	10	100	700	30	200	260	260	280	89.5	\approx straight

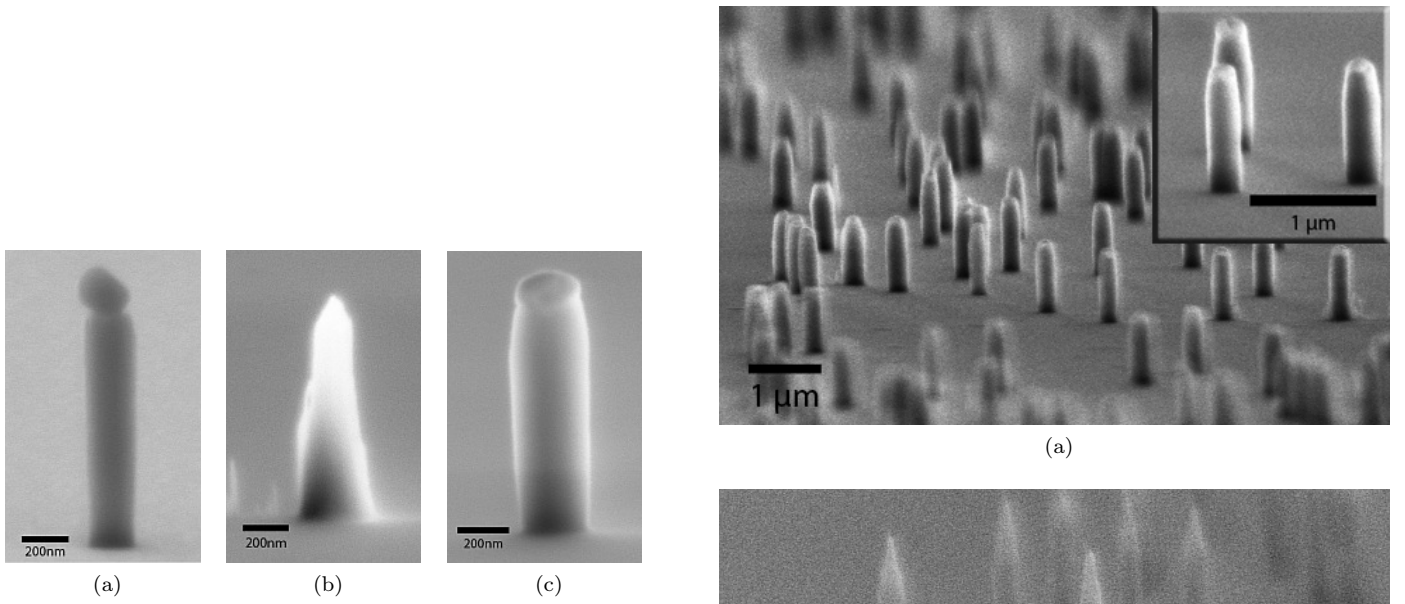


Figure 5: Poly-D nanowires obtained with (a) Al_2O_3 powder (≈ 200 nm in diameter), (b) SiO_2 particles (210 nm in diameter) and (c) 250 nm gold particles as mask, etched with the oxygen recipe. (a) The height is $\approx 1 \mu\text{m}$ and the diameter is 200 nm both on the top and the bottom. The thickest diameter is 230 nm. The particle height is ≈ 210 nm and its thickest diameter is 230 nm. (b) The height of the wires is $1 \mu\text{m}$ and the diameter varies from ≈ 342 nm on the bottom to ≈ 20 nm at the top. (c) The nanowire is ≈ 900 nm high. The diameter varied from 275 nm on the bottom, to a maximum of 310 nm and 250 nm at the top. The particle measures 245 nm in diameter and 130 nm in height. The etch time was 5 min.

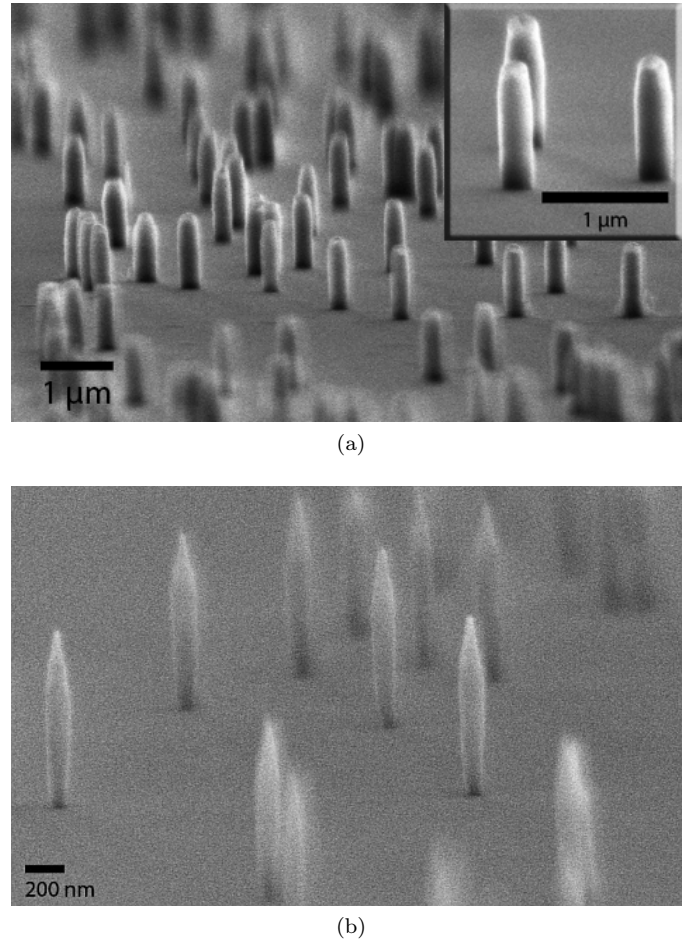


Figure 6: Poly-D nanowires after a 5 min oxygen etch. (a) 250 nm-Au colloids served as etch mask. The top-bottom height of the wires is $\approx 1 \mu\text{m}$ and the thickest diameter is about 280 nm. The diameter at the bottom of the wires is ≈ 260 nm. Inset: Close-up view of some wires. Figure (b) shows poly-D nanowires obtained with a 1:200 dilution of 100 nm-Au colloids as a mask. The top-bottom height of the wires is $\approx 0.9 \mu\text{m}$ and the thickest diameter is about 120 nm.

4.3. Single crystal diamond nanowires

Due to the ease in dispersing and the reasonable etch selectivity of 8:1, Au nanoparticles were drop-casted on E6 CVD IIa and E6 HPHT Ib samples. The samples were etched for 5 min and 10 min, respectively, the results of which are shown in Figure 7. After a 5 min etch, the nanowires are broadened in the bottom half and are almost straight in the upper half, as indicated in Figure 7a. The top-bottom wire height is $\approx 1.1 \mu\text{m}$. The diameters vary from $\approx 350 \text{ nm}$ at the bottom of the wires to $\approx 230 \text{ nm}$ at the top just beneath the remaining particles. The etching time was 5 min. An etch rate of 220 nm/min was measured. Ib sc-D nanowires after a 10 min etch are shown in Figure 7b. The gold particle mask was almost completely eroded after this time and thus the upper part of the nanowire comes out tapered. The etch rate is 190 nm/min . The top-bottom height is $\approx 1.9 \mu\text{m}$ and the diameters vary from $\approx 470 \text{ nm}$ at the bottom of the wires to $\approx 190 \text{ nm}$ at the top beneath the remaining particles. The mask etch rate was in both cases $20 - 25 \text{ nm/min}$. Thus the etch selectivity was found to be $\approx 8 : 1$ and $\approx 9 : 1$ for Ib and IIa sc-Ds respectively.

While the nanoparticle drop-casting approach provides a simple method to realize a large number of randomly positioned diamond nanowires, ordered arrays of nanowires are desirable for the characterization of functional devices. Another factor to consider is the effect of the near-spherical shape of the nanoparticle etch mask on the etch profile of nanowires. Due to these reasons, EBL-defined masks have also been considered in this work.

Ordered arrays of varying diameters between 100 nm and 250 nm , which covers the range of the optimum diameters as presented in Section 2, were patterned on sc-D samples. Wire-to-wire distances (periodicity) of $2 \mu\text{m}$ and $3 \mu\text{m}$ were used. The distance was chosen to allow ease in characterization of individual nanowires using a custom built confocal micro- photoluminescence setup without introducing any stray signal from neighboring nanowires. Details of the experimental setup and results will be presented in a future publication.

EBL using PMMA resists followed by a lift-off process was used to realize an evaporated Cr/Au metal mask, as described in Section 3 (Figure 3). The results of etching E6 IIa CVD diamond with such a mask are shown in Figure 8. A 10 min oxygen etch produces $2.2 \mu\text{m}$ high nanowires. The diameter at the top of the wires of this array is $\approx 160 \text{ nm}$ and at the bottom $\approx 490 \text{ nm}$. The diamond etch rate is 220 nm/min , whereas the etch rate of the evaporated gold is 26 nm/min . In the inset a wire is shown with the remaining mask after a 5 min etch. The mask is $\approx 120 \text{ nm}$ high and the diameter of the wire is $\approx 200 \text{ nm}$ at the top. Again, an over cut etch profile is observed in the case of sc-D nanowires. As mentioned above, the same recipe resulted in a vertical nanowire profile in the case of poly-D nanowires. We expect that an increase in the isotropic etch component of our recipe would result in straighter nanowires.

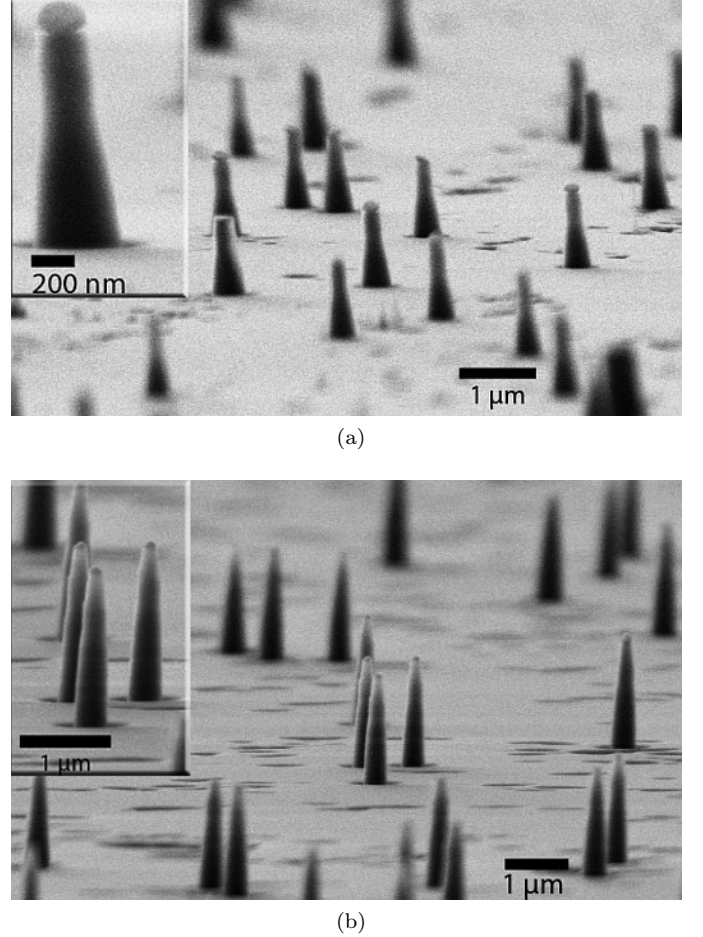


Figure 7: Sc-D nanowires obtained with 250-nm-Au colloids as a mask for oxygen etching. (a) E6 IIa sc-D nanowires with a top-bottom wire height of $\approx 1.1 \mu\text{m}$. The diameters vary from $\approx 350 \text{ nm}$ at the bottom of the wires to $\approx 230 \text{ nm}$ at the top. The etching time was 5 min. Inset: Close-up view of one wire. (b) E6 Ib nanowires with a top-bottom height of $\approx 1.9 \mu\text{m}$. The diameters vary from $\approx 470 \text{ nm}$ at the bottom of the wires to $\approx 190 \text{ nm}$ at the top beneath the remaining particles. The etching time was 10 min. Inset: Magnified view of three wires.

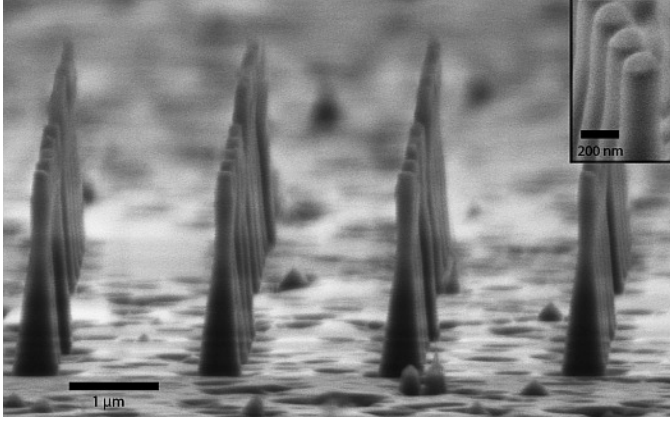


Figure 8: Sc-D nanowires obtained in a IIa CVD diamond. After a 10 min oxygen etch using an EBL defined evaporated Cr/Au (10/200)nm mask. The height is $2.2\text{ }\mu\text{m}$ from top to bottom, the remaining mask on this set of wires is $\approx 60\text{ nm}$ high. The diameter just beneath the mask is $\approx 160\text{ nm}$ and at the bottom $\approx 490\text{ nm}$. Inset: The etch time was 5 min, the remaining mask on this set of wires is $\approx 120\text{ nm}$ high. The diameter just beneath the mask is $\approx 200\text{ nm}$.

Au nanoparticles and evaporated Au gave a similar etch rate of 25 nm/min . In order to further simplify the fabrication procedure, we used FOx (which is a negative e-beam resist) as an etch mask, as mentioned in Section 3 (Figure 3). This required no metal evaporation and lift-off. The profile of the wires in E6 Ib sc-D can be seen in Figure 9. Figure 9a shows $2.3\text{ }\mu\text{m}$ high wires. The EBL-written diameter of this array was 150 nm . The measured diameters at the broadest part of the top and the bottom are $\approx 110\text{ nm}$ and $\approx 310\text{ nm}$, respectively. At the thinnest part of the wires the diameter is $\approx 70\text{ nm}$. In Figure 9c, an array of $2.2\text{ }\mu\text{m}$ high nanowires with a bottom diameter of 226 nm are shown (written diameter: 100 nm). We found the etch rate of FOx to be smaller than 10 nm/min , which is almost three times better than the metal mask.

In order to improve the etch profile of sc-D nanowires and obtain nanowires with vertical sidewalls, we changed our etch recipe slightly by varying the ICP power. Based on the profile we obtained with our base etch recipe, we decided to decrease the chemical etch rate after a few minutes and then increase it to prevent the broadening of the wires (Figures 8 and 9). We used our usual recipe for 2 min, decreased the ICP power to 600 W for 3 min and then ramped up to 1000 W for 5 min. The results can be seen in Figure 10a. The periodicity and diameter of the wires used in EBL are $3\text{ }\mu\text{m}$ and 200 nm respectively. We were able to realize $1.9\text{ }\mu\text{m}$ tall nanowires with near vertical profile (bottom diameter of $\approx 260\text{ nm}$) and a tapered top due to the high ICP power causing mask erosion. This can be minimized by using a thicker FOx mask film. As mentioned earlier, however, a tapered profile may be preferable [16] for increasing the extraction collection efficiency from

emitters embedded inside nanowires.

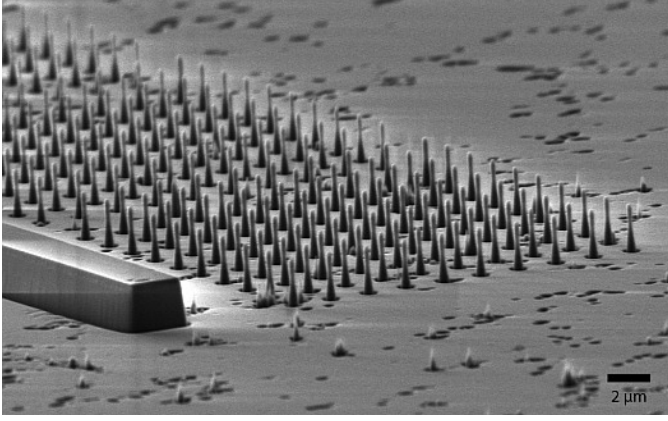
Based on the above recipe optimization results, an ultra pure type IIa diamond from Apollo Diamond, Inc. was also etched with slightly different etch step lengths: 1.5 min, 3 min and 5.5 min. The profile of the $2.4\text{ }\mu\text{m}$ tall wires with a periodicity of $3\text{ }\mu\text{m}$ can be seen in Figures 10b and 10c. Nanowires with a bottom diameter of 340 nm are shown in Figure 10b (EBL written diameter: 220 nm). The thinnest and top diameters are 190 nm and $210\text{ }\mu\text{m}$ respectively. Another array with diameters ranging from 170 nm at the bottom to 60 nm at the nanowire waist and 120 nm at the top can be seen in Figure 10c. The diameter used in EBL was 140 nm . The wire etch rate was measured as 240 nm/min .

Table 2: Summary of the etch rates in the different diamond types. For the Apollo IIa a different etch recipe has been used (see section 4.3), for the other diamond types we used the etch recipe introduced in section 3.

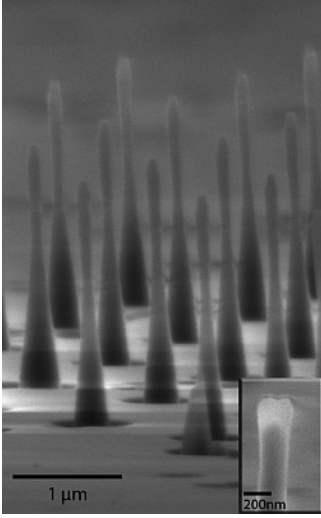
Type	Etch rate nm/min	etch time min
poly-D	200	5
Ib sc-D	190	10
IIa sc-D (E6)	220	5
IIa sc-D (Apollo Diamond)	240	10

5. Conclusion

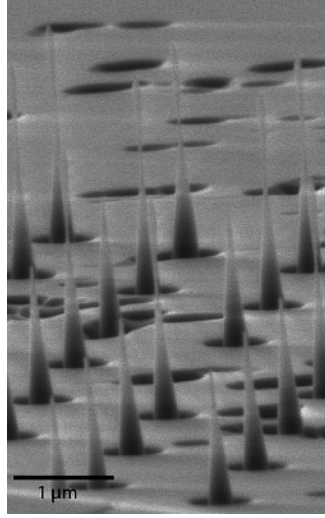
In this work, we have presented the design and fabrication of diamond nanowires. Our modeling shows an optimal range of diameters for coupling ($>80\%$) the Nitrogen Vacancy (NV) center emission to the propagating waveguide mode inside the diamond nanowire, and collecting that emission with a high extraction efficiency using a 0.95 NA objective. We have also investigated diamond etching of poly-D and sc-D nanowires. We have summarized the etch rates of all diamond types in table 2. Nanowires with near vertical profiles were fabricated using an oxygen ICP RIE recipe. Al_2O_3 , Au and SiO_2 particles, evaporated Au and FOx e-beam resist were evaluated as an etch mask. It was found that Al_2O_3 nanoparticles were most resistant to etching. Au nanoparticles and evaporated Au gave a similar etch rate, while FOx e-beam resist gave an etch rate of 10 nm/min and was found to be the most suitable mask based on our fabrication process. The crystalline nature of the samples affected the etch profile and required different etch parameters to obtain nearly vertical etch profiles of the nanowires. Polycrystalline and type Ib single crystal diamond were found to etch at $(190 - 200)\text{ nm/min}$, whereas type IIa single crystal diamonds were found to etch at about $(220 - 240)\text{ nm/min}$. We believe that our nanowire work and the diamond nanophotonic technology that we are developing will play an important role as an enabling platform for fundamental quantum information



(a)

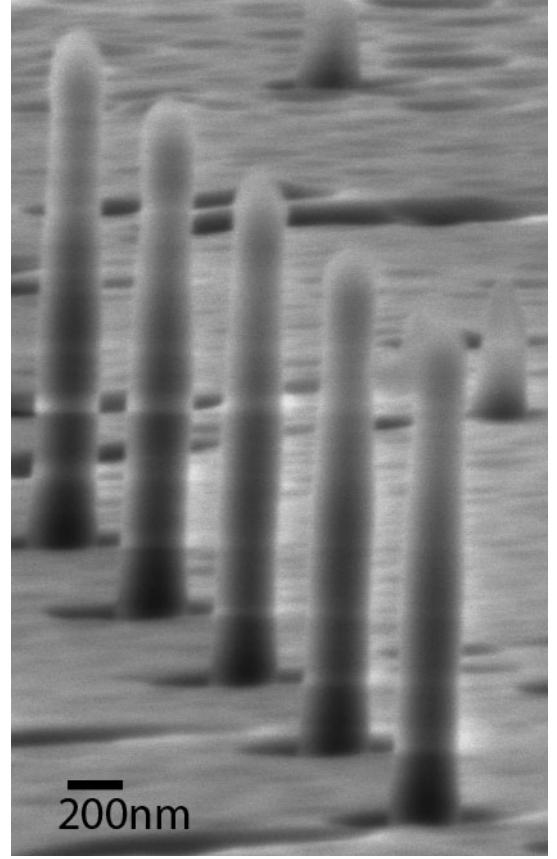


(b)

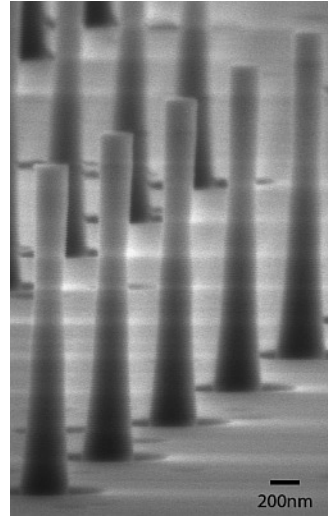


(c)

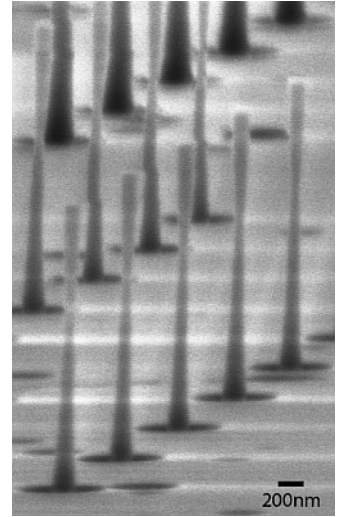
Figure 9: Sc-D wires formed in a 1b HPHT diamond. FOx was used to produce an array of pillar-shaped mask with EBL. The mask was then transferred to the substrate during a 10 min oxygen etch and subsequently removed. (a) One pattern of wires with the same diameters. (b) The height of the wires is $2.3\text{ }\mu\text{m}$ from top to bottom. The diameters at the broadest part of the top and the bottom are $\approx 110\text{ nm}$ and $\approx 310\text{ nm}$ respectively. At the thinnest part of the wires the diameter is $\approx 70\text{ nm}$. Inset: One wire with the remaining FOx mask after etching (different diameter). (c) One array of $2.2\text{ }\mu\text{m}$ high nanowires with a bottom diameter of 226 nm .



(a)



(b)



(c)

Figure 10: (a) Sc-D (1b HPHT) wires after a 10 min oxygen etch. The FOx mask was removed. The height of the wires is $1.9\text{ }\mu\text{m}$ from top to bottom and the diameter at the bottom is $\approx 260\text{ nm}$. (b) and (c) Sc-D nanowires formed in a diamond from Apollo Diamond after removing the FOx mask. Their height is $2.4\text{ }\mu\text{m}$ and the distance between each nanowire is $3\text{ }\mu\text{m}$. (b) Nanowires with a bottom diameter of 340 nm . The thinnest and top diameters are 190 nm and 210 nm respectively. (c) The diameter varies from 170 nm at the bottom, to 60 nm at the nanowire waist and 120 nm at the top.

processing applications, as well as bio-sensing applications based on magnetometry [30].

6. Acknowledgments

This work is supported in part by the DARPA Quest program (PM Jagdeep Shah), NSF NIRT grant, and Harvard NSEC. The authors wish to acknowledge the help during the search for a suitable nanowire fabrication process by Chih-Hsun Hsu and Jeffrey Shainline (Jimmy Xu's lab at Brown University). The authors thank Advanced Diamond Technologies and Apollo Diamond for providing diamond test samples. Fruitful discussions with Philippe Lalanne and help from Maja Cassidy and Ben Hatton are acknowledged. One of the authors (B. H.) wishes to cordially thank Anna Fontcuberta i Morral and Jonathan Finley for their support. Most of the fabrication work was performed at the Center for Nanoscale Sciences (CNS) Nanofabrication facility at Harvard University, a member of the National Nanotechnology Infrastructure Network (NNIN), which is supported by the National Science Foundation under NSF award no. ECS-0335765. Disclaimer: The views, opinions, and/or findings contained in this publication are those of the authors and should not be interpreted as representing the official views or policies, either expressed or implied, of the Defense Advanced Research Projects Agency or the Department of Defense..

References

- [1] C. Kurtsiefer, S. Mayer, P. Zarda, and H. Weinfurter, "Stable solid-state source of photons", *Phys. Rev. Lett.* **85**, 290-293 (2000).
- [2] N. Reddy, N. Manson and E. Krausz, "Two-laser spectral hole burning in a color center in diamond", *J. Lumin.* **38**, 46-47 (1987).
- [3] F. Jelezko, C. Tietz, A. Gruber, I. Popa, A. Nizovtsev, S. Kilin and J. Wrachtrup, "Spectroscopy of single N-V centers in diamond", *Single Mol.* **2**, 255-260 (2001).
- [4] T. Gaebel, M. L. Domhan, I. Popa, C. Wittmann, P. Neumann, F. Jelezko, J. R. Rabeau, N. Stavrias, A. D. Greentree, S. Prawer, J. Meijer, J. Twamley, P. R. Hemmer, and J. Wrachtrup, "Room-temperature coherent coupling of single spins in diamond", *Nat. Phys.* **2**, 408-413 (2006).
- [5] J. W. Baldwin, M. K. Zalalutdinov, T. Feygelson, J. E. Butler, and B. H. Houston, "Fabrication of short-wavelength photonic crystals in wide-band-gap nanocrystalline diamond films", *J. Vac. Sci. Technol. B* **24**, 50-54 (2006).
- [6] C. F. Wang, Y.-S. Choi, J. C. Lee, E. L. Hu, J. Yang, and J. E. Butler, "Observation of whispering gallery modes in nanocrystalline diamond microdiscs", *Appl. Phys. Lett.* **90**, 081110 (2007).
- [7] C.F. Wang, R. Hanson, D.D. Awschalom, E.L. Hu, T. Feygelson, J. Yang, and J.E. Butler, "Fabrication and characterization of two-dimensional photonic crystal microcavities in nanocrystalline diamond", *Appl. Phys. Lett.* **91**, 201112 (2007).
- [8] P. Olivero, S. Rubanov, P. Reichart, B. C. Gibson, S. T. Huntington, J. Rabeau, A. D. Greentree, J. Salzman, D. Moore, D. N. Jamieson, and S. Prawer, "Ion-Beam-Assisted Lift-Off Technique for Three-Dimensional Micromachining of Freestanding Single-Crystal Diamond", *Adv. Mater.*, **17**,
- [9] M. P. Hiscocks, K. Ganesan, B. C. Gibson, S. T. Huntington, F. Ladouceur, and S. Prawer, "Diamond waveguides fabricated by reactive ion etching", *Opt. Express* **16** (24), 19512-19519 (2009).
- [10] C. F. Wang, and E. L. Hu, "Fabrication of suspended single crystal diamond devices by electrochemical etch", *J. Vac. Sci. Technol. B*, **25** (3), 730-733 (2007). 2427-2430 (2005).
- [11] K.-M. C. Fu, P. E. Barclay, I. Aharonovich, S. Prawer, A. M. Holm, and R. G. Beausoleil, "Coupling of nitrogen-vacancy centers in diamond to a GaP waveguide", *Appl. Phys. Lett.* **93** 234107 (2008).
- [12] M. W. McCutcheon, and M. Lončar, "Design of an ultrahigh Quality factor silicon nitride photonic crystal nanocavity for coupling to diamond nanocrystals", *Opt. Express* **16**, 19136 (2008).
- [13] K. Rivoire, A. Faraon, and J. Vučković, "Gallium phosphide photonic crystal nanocavities in the visible", *Appl. Phys. Lett.* **93**, 063103 (2008).
- [14] P. E. Barclay, O. Painter, C. Santori, K.-M. Fu, and R. G. Beausoleil, "Coherent interference effects in a nano-assembled optical cavity-QED system", arXiv:0812.4505, (2008).
- [15] S. Schietinger, M. Barth, T. Aichele, and O. Benson, "Plasmon Enhanced Single Photon Emission from a Nanoassembled Metal-Diamond Hybrid Structure at Room Temperature", *Nano Lett.* **9** (4), 1694-1698 (2009).
- [16] I. Friedler, C. Sauvan, J. P. Hugonin, P. Lalanne, J. Claudon, and J. M. Gérard, "Solid-state single photon sources: the nanowire antenna", *Opt. Express* **17**, 2095-2110 (2009).
- [17] Y. Ando, Y. Nishibayashi, and A. Sawabe, "Nano-rods' of single crystalline diamond", *Diam. Relat. Mater.* **14**, 633-637 (2004).
- [18] C. L. Lee, E. Gu, M. D. Dawson, I. Friel, and G. A. Scarsbrook, "Etching and micro-optics fabrication in diamond using chlorine-based inductively-coupled plasma", *Diam. and Relat. Mater.* **17**, 1292-1296 (2008).
- [19] E. Gu, H. W. Choi, C. Liu, C. Griffin, J. M. Girkin, I. M. Watson, M. D. Dawson, G. McConnell, and A. M. Gurney, "Reflection/transmission confocal microscopy characterization of single-crystal diamond microlens arrays", *Appl. Phys. Lett.* **84** (15), 2754-2756 (2004).
- [20] H. Shiomi, "Reactive ion etching of diamond in O₂ and CF₄ plasma, and fabrication of porous diamond for field emitter cathodes", *Jpn. J. Appl. Phys.* **36**, 7745-7748 (1997).
- [21] T. Yamada, P. R. Vinod, D.-S. Hwanga, H. Yoshikawa, S. Shikata and N. Fujimori, "Self-aligned fabrication of single crystal diamond gated field emitter array", *Diam. and Relat. Mater.* **14**, 2047-2050 (2005).
- [22] T. Yamada, H. Yoshikawa, H. Uetsuka, S. Kumaragurubaran, N. Tokuda, S. Shikata, "Cycle of two-step etching process using ICP for diamond MEMS applications", *Diam. and Relat. Mater.* **16**, 996-999 (2007).
- [23] D. Hwang, T. Saito and N. Fujimori, "New etch process for device fabrication using diamond", *Diam. and Relat. Mater.* **13**, 2207-2210 (2004).
- [24] M. Larsson, K. N. Dinyari, and H. Wang, "Composite optical microcavity of diamond nanopillar and silica microsphere", *Nano Lett.* **9** (4), 1447-1450 (2009).
- [25] Y. Ando, Y. Nishibayashi, K. Kobashi, T. Hirao, and K. Oura, "Smooth and high-rate reactive ion etching of diamond", *Diam. and Relat. Mater.* **11**, 824-827 (2002).
- [26] J. W. Baldwin, M. K. Zalalutdinov, T. Feygelson, B. B. Pate, J. E. Butler, and B. H. Houston, "Nanocrystalline diamond resonator array for RF signal processing", *Diam. and Relat. Mater.* **15**, 2061-2067 (2006).
- [27] A. V. Maslov, and C. Z. Ning, "Far-field emission of a semiconductor nanowire laser", *Opt. Lett.* **26** (6), 572-574 (2004).
- [28] J. Vučković, D. Fattal, C. Santori, G.S. Solomon, and Y. Yamamoto, "Enhanced single-photon emission from a quantum dot in a micropost microcavity", *Appl. Phys. Lett.* **82** (21) (2003).
- [29] N. Gregersen, T. R. Nielsen, J. Claudon, J.-M. Gérard, and J. Mørk, "Controlling the emission profile of a nanowire with a conical taper", *Opt. Lett.* **33** (15), 1693-1695 (2008).
- [30] J. R. Maze, P. L. Stanwix, J. S. Hodges, S. Hong, J. M. Taylor, P. Cappellaro, L. Jiang, M. V. Gurudev Dutt, E. Togan, A. S. Zibrov, A. Yacoby, R. L. Walsworth, and M. D. Lukin, "Nanoscale magnetic sensing with an individual electronic spin in diamond", *Nat.* **455**, 644-648 (2008).